Numerical Modeling for the H_2/CO Bluff-Body Stabilized Flames

Seong-Ku Kim, Yong-Mo Kim*
Department of Mechanical Engineering, Hanyang University
Kook-Young Ahn, Koonsup Oh
Korea Institute of Machinery and Materials

This study investigates the nonpremixed H_2/CO-air turbulent flames numerically. The turbulent combustion process is represented by a reaction progress variable model coupled with the presumed joint probability function. In the present study, the turbulent combustion model is applied to analyze the nonadiabatic flames by introducing additional variable in the transport equation of enthalpy and the radiative heat loss is calculated using a local, geometry independent model. Calculations are compared with experimental data in terms of temperature, and mass fraction of major species, radical, and NO. Numerical results indicate that the lower and higher fuel-jet velocity flames have the distinctly different flame structures and NO formation characteristics in the proximity of the outer core vortex zone. The present model correctly predicts the essential features of flame structure and the characteristics of NO formation in the bluff-body stabilized flames. The effects of nonequilibrium chemistry and radiative heat loss on the thermal NO formation are discussed in detail.

Key Words : Bluff-Body Stabilized Flames, Nonpremixed H_2/CO Turbulent Flames, Thermal NO Formation, Numerical Modeling, Nonequilibrium Chemistry, Radiation Effect

1. Introduction

The bluff-body combustors have been widely used in many engineering applications. The bluff-body stabilized flows have been investigated experimentally and theoretically (Correa, 1994; Masri, 1996, Combustion data base; TNF workshop proceeding, 1998) because this type of flame field has the excellent turbulent mixing characteristics and improved flame stability. Beside these practical interest, the bluff-body stabilized flames are very useful to study the interaction between turbulence and chemistry in the turbulent recirculating reactive flows. Due to its simple and well-defined boundary conditions as well as its ability to maintain the flame stabilization for a wide range of inlet flow conditions, the bluff-body stabilized flames are now the popular subject for combustion laser diagnostics and modeling.

Even though understanding of combustion processes has advanced significantly by recent progress in the combustion modeling (TNF workshop proceeding) and laser diagnostic technology (Masri, 1996), the prediction of combustion processes and pollutant formation in the chemically reacting flow system still remains in the challenging problems mainly due to the complex chemistry-flow interaction. In dealing with the well-known closure problem for modeling mean chemical reaction rates, the turbulent combustion models are largely classified as the presumed joint pdf methods (Janicka, 1982; Correa, 1984; Biagioli, 1997; Louis, 1997; Kok, 1998) and the pdf transport methods (Biagioli, 1997; Correa,

* Corresponding Author
E-mail : ymkim@email. hanyang. ac. kr
TEL : +82-2-2290-0428; **FAX** : +82-2-2297-0339
Department of Mechanical Engineering, Hanyang University, 17, Haengdang-dong, Sungdong-ku, Seoul 133-791, Korea. (Manuscript **Received** December 22, 1999; **Revised** May 19, 2000)

1994). In the presumed pdf methods, the mean chemical source terms and the ensemble-averaged properties of the reacting mixture are evaluated by convoluting the instantaneous properties with the assumed joint probability distribution. This approach has difficulties to prescribe the correct analytical function for the joint pdf which is dependent on the hydrodynamics of the turbulent flame field. On the other hand, the pdf transport model has the basic advantage to handle the chemical source terms of the species transport equations without modeling. Thus this model does not require the high Damkohler number assumption and is applicable to the flame field with the broad chemical time scales. However the pdf transport model has the major difficulties in modeling the molecular mixing as well as in representing the thin reaction zone. Moreover a large number of computational particles is needed for the realistic representation of statistics and the numerical convergence in the Monte Carlo Simulation.

In order to attain the reliable prediction of the combustion processes and the emission characteristics for the practical combustors, the turbulent combustion model needs to be numerically efficient as well as to be physically realistic. Even if the pdf transport methods are applicable to the flame fields with the broad chemical time scales and it is often acknowledged to be superior to the presumed joint pdf methods, their required computational time even for the simple flames (Biagioli, 1997) is formidably longer than the RPV model coupled with the presumed joint pdf. In the aspect of design applications, the RPV model is regarded as one of the practically optimal choices between accuracy and computational efficiency.

In context with the RPV model, the early modeling of the turbulent hydrogen jet flames was initiated with Janicka and Kollmann's work (Janicka, 1982). They suggested the reaction progress variable (RPV) model adopting the slow three-body recombination of radicals and the partial equilibrium assumptions for the fast two shuffle reactions, and revealed that their RPV model was capable of predicting the superequilibrium concentrations of free radicals. Later, Correa (Correa, 1984) applied the RPV model to analyze the nonpremixed CO/H_2 flame by including CO into a hydrogen reaction progress variable. Biagioli (Biagioli, 1997) addressed the utilities of RPV model in comparison with the PDF transport model for bluff-body stabilized flames. Recently, Kok and Louis (Louis, 1997; Kok, 1998) improved the predicative capability of the RPV model for analyzing the syngas flames. This improved RPV model can account for the effect of the HO_2 and H_2O_2 chemistry which is important for the lean mixtures and the moderate temperature. Their results indicated that the incorporation of the additional species yielded the more accurate prediction of the nonequilibrium departure from the equilibrium hydrogen chemistry. Moreover, their RPV model was extended to incorporate the nonadiabatic flame conditions by introducing the enthalpy transport variable. Kok and Louis (Louis, 1997; Kok, 1998) applied their RPV model to analyze the syngas flame. However this modified RPV model has not been extensively validated against the benchmark cases with the detailed experimental data of the local flame properties.

The present study employs the improved RPV model (Louis, 1997; Kok, 1998) to predict the flame structure and pollutant formation of the H2/CO-air bluff-body stabilized flames for which detailed experimental data (Masri, 1996; Combustion data base) are available. The predicative capability of the RPV combustion model has been validated against the detailed experimental data involving the distribution of temperature, major species, radicals, and NO. Special emphasis is given to effects of nonequilibrium chemistry, radiative heat transfer, and fuel jet velocity on the flame structure and the thermal NO formation.

2. Physical Models

2.1 Chemistry model

The chemistry model used in the present study is based on the combustion mechanism of H2/CO-air (Warnatz, 1996) shown in Table 1. This reaction mechanism is characterized by three

Table 1 Reaction mechanism for H_2/CO-air combustion (unit: mol, cm, s, K, kJ)

	Reaction	A	b	E
R1	$H+O_2=OH+O$	2.00E14	0.00	70.30
R2	$H_2+O=OH+H$	5.06E04	2.67	26.30
R3	$H_2+OH=H_2O+H$	1.00E08	1.60	13.80
R4	$OH+OH=H_2O+O$	1.50E09	1.14	0.42
R5	$H+H+M=H_2+M$	1.80E18	-1.00	0.00
R6	$H+OH+M=H_2O+M$	2.20E22	-2.00	0.00
R7	$O+O+M=O_2+M$	2.90E17	-1.00	0.00
R8	$H+O_2+M=HO_2+M$	2.30E18	-0.80	0.00
R9	$HO_2+H=OH+OH$	1.50E14	0.00	4.20
R10	$HO_2+H=H_2+O_2$	2.50E13	0.00	2.90
R11	$HO_2+H=H_2O+O$	3.00E13	0.00	7.20
R12	$HO_2+O=OH+O_2$	1.80E13	0.00	-1.70
R13	$HO_2+OH=H_2O+O_2$	6.00E13	0.00	0.00
R14	$HO_2+HO_2=H_2O_2+O_2$	2.50E11	0.00	-5.20
R15	$OH+OH+M=H_2O_2+M$	3.25E22	-2.00	0.00
R16	$H_2O_2+H=H_2+HO_2$	1.70E12	0.00	15.70
R17	$H_2O_2+H=H_2O+OH$	1.00E13	0.00	15.00
R18	$H_2O_2+O=OH+HO_2$	2.80E13	0.00	26.80
R19	$H_2O_2+OH=H_2O+HO_2$	5.40E12	0.00	4. 20
R20	$CO+OH=CO_2+H$	6.00E06	1.50	-3.10
R21	$CO+O+M=CO_2+M$	7.10E13	0.00	-19.00

reaction processes involving the fast shuffle reactions (R1～R4, R20), the three-body recombinations (R5～R7, R21), and the HO_2/H_2O_2 chemistry (R8～R13, R14～R19). According to the previous studies (Janicka, 1982; Correa, 1984; Biagioli, 1997), the fast shuffle reactions (R1～R4, R20) forming the radicals, O, H and OH are assumed to be in partial equilibrium while this radical pool decays slowly by progress of the three-body recombinations (R5～R7, R21) to reach an equilibrium. The reaction system (R1～R7, R20～R21) neglecting HO_2/H_2O_2 chemistry might provide the reasonable results at high temperatures and conditions close to stoichiometry. However, as Kok and Louis (Louis, 1997; Kok, 1998) pointed out, for moderate temperatures and lean mixtures, the reactions (R8～R19) involving HO_2 and H_2O_2 species become progressively important. Since this HO_2/H_2O_2 chemistry enhances the decay rate of the radical pool by yielding the extra reaction path, compared to the reaction system (R1～R7, R20～R21) neglecting the HO_2/H_2O_2 chemistry, the combustion proceeds to the reaction state much closer to equilibrium. Therefore, the omission of these additional reactions of HO2 and H_2O_2 leads to the overestimated departure from equilibrium. In the present formulation, the combined variable $Y^*_{H_2}$ corresponding to the full reaction system (R1～R21) is introduced to include the effect of additional species HO_2 and H_2O_2.

$$Y^*_{H_2}=Y_{H_2}+\frac{M_{H_2}}{M_O}Y_O+\frac{3}{2}\frac{M_{H_2}}{M_H}Y_H+\frac{1}{2}\frac{M_{H_2}}{M_{OH}}Y_{OH}+\frac{M_{H_2}}{M_{CO}}Y_{CO}-\frac{1}{2}\frac{M_{H_2}}{M_{HO_2}}Y_{HO_2}-\frac{M_{H_2}}{M_{H_2O_2}}Y_{H_2O_2} \tag{1}$$

The source term for the combined variable $Y^*_{H_2}$ is determined only by the three-body reactions without activation energy.

$$\dot{w}^*_{H_2}=-2M_{H_2}(w_5+w_6+w_7+w_8+w_{15}+w_{21}) \tag{2}$$

Five equations arise from the partial equilibrium assumptions for the fast reactions (R1～R4, R20):

$$\frac{Y_{OH}Y_O}{Y_HY_{O_2}}=K_{c1}\frac{M_{OH}M_O}{M_HM_{O_2}}=G_1(T) \tag{3}$$

$$\frac{Y_{OH}Y_H}{Y_OY_{H_2}}=K_{c2}\frac{M_{OH}M_H}{M_OM_{H_2}}=G_2(T) \tag{4}$$

$$\frac{Y_{H_2O}Y_H}{Y_{H_2}Y_{OH}}=K_{c3}\frac{M_{H_2O}M_H}{M_{H_2}M_{OH}}=G_3(T) \tag{5}$$

$$\frac{Y_{HO}Y_O}{Y_{OH^2}}=K_{c4}\frac{M_{H_2O}M_O}{M_{OH^2}}=G_4(T) \tag{6}$$

$$\frac{Y_{CO_2}Y_H}{Y_{CO}Y_{OH}}=K_{c20}\frac{M_{CO_2}M_H}{M_{CO}M_{OH}}=G_{20}(T) \tag{7}$$

In these equations Kci is the equilibrium constant for matching reactions.

Only four of five reactions are independent, so four algebraic equations can be used as follows:

$$Y_O=(G_1\ G_3)\cdot\frac{Y_{H_2}Y_{O_2}}{Y_{H_2O}} \tag{8}$$

$$Y_H=\left(G_1^{\frac{1}{2}}\ G_3^{\frac{1}{2}}\ G_4^{-\frac{1}{2}}\right)\cdot\frac{Y_{H_2}^{\frac{1}{2}}Y_{O_2}^{\frac{1}{2}}}{Y_{H_2O}} \tag{9}$$

$$Y_{OH}=\left(G_1^{\frac{1}{2}}\ G_3^{\frac{1}{2}}\ G_4^{-\frac{1}{2}}\right)\cdot Y_{H_2}^{\frac{1}{2}}Y_{O_2}^{\frac{1}{2}} \tag{10}$$

$$Y_{CO}=(G_3\ G_{20}^{-1})\cdot\frac{Y_{H_2}\ Y_{CO_2}}{Y_{H_2O}} \tag{11}$$

Therefore, based on the partial equilibrium assumption, the radical concentrations can be expressed in terms of the concentrations of major species.

And the species HO_2 and H_2O_2 are assumed to be in steady state and therefore the following relations have to be satisfied :

$$w_8-w_9-w_{10}-w_{11}-w_{12}-w_{13}-2w_{14}+w_{16}+w_{18}+w_{19}=0 \quad (12)$$

$$w_{14}+w_{15}-w_{16}-w_{17}-w_{18}-w_{19}=0 \quad (13)$$

With equal diffusivity assumption, the mixture fraction is defined as:

$$f=\frac{\phi-\phi_a}{\phi_f-\phi_a},\ \phi=Z_H,\ Z_O,\ Z_C,\ Z_N \quad (14)$$

where, Z_i denotes the mass fraction of element i.

2.2 Extension to nonadiabatic flame

When the radiative heat loss is taken into account, enthalpy transport is no longer described by the mixture fraction transport equation. Thus, in numerical modeling the nonadiabatic flame field, a transport equation for separate enthalpy variable must be solved. A normalized enthalpy variable (Louis, 1997) is utilized for improving statistical independence from the mixture fraction as well as for convenience in generating lookup table:

$$e=\frac{h-h_{min}}{h_{ad}-h_{min}}=\frac{h-h_{min}}{U(f)} \quad (15)$$

Here, h and h_{ad} are the total static enthalpy and the adiabatic enthalpy, respectively. h_{min} is defined as the minimum enthalpy of the mixture corresponding to the surrounding temperature. h_{ad} and h_{min} are dependent only on the mixture fraction. Since the composition of the burnt mixture depends on enthalpy variable and mixture fraction, the reaction progress variable for the nonadiabatic flames is introduced to account for the effects of the radiative cooling.

$$r=\frac{Y^*_{H_2}-Y^*_{H_2}{}^{ub}}{Y^*_{H_2}{}^{eq}-Y^*_{H_2}{}^{ub}}=\frac{Y^*_{H_2}-Y^*_{H_2}{}^{ub}}{W(f,\ e)} \quad (16)$$

where the superscripts eq and ub denote equilibrium and unburned mixtures, respectively.

The instantaneous thermochemical state of a mixture in a nonpremixed flame can now be determined by three variables, f, r, and e which describe mixing process, nonequilibrium chemistry, and deviation from adiabatic condition, respectively. Prior to a flame calculation, all the thermochemical properties such as temperature, species concentrations, density, and the source term of each transport equation are calculated in the allowable ranges of f, r and e, and these calculated data are stored in a lookup table. Figure 1 shows the distributions of temperature and O radical mass fraction at adiabatic condition ($e=1$) within the lookup table constructed for the flame condition in which the fuel consisting of 66.67% H_2 and 33.33% CO by volume reacts with air and the corresponding value of stoichiometric mixture fraction is 0.1350. The

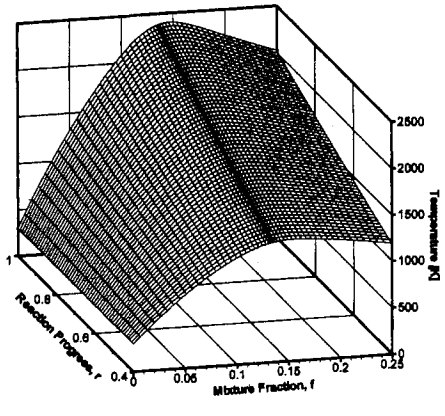

(a) Temperature

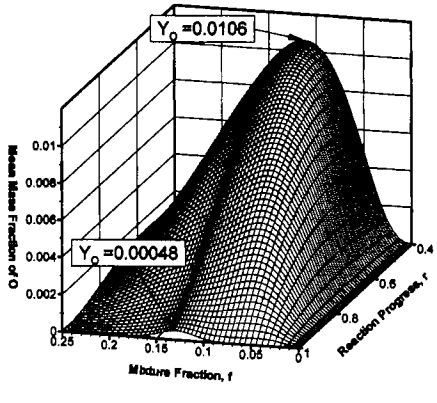

(b) O radical mass fraction

Fig. 1 The f-r plane data base of temperature and O radical mass fraction at adiabatic(e=1)

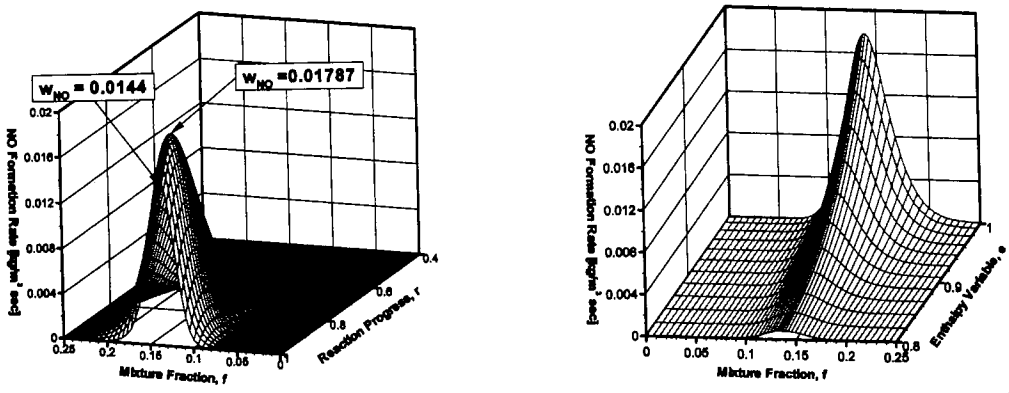

(a) NO formation rate in the f-r plane at e=1

(b) NO formation rate in f-e plane at r=0.95

Fig. 2 The data base of thermal NO formation rate in the f-r plane at e=1 and in the f-e plane at r=0.95

maximum temperature occurs at equilibrium (r=1) near the stoichiometry, while O radical mass fraction has the super-equilibrium peak which is about twenty times larger than the peak value at equilibrium state.

The present study assumes that the flame is optically thin so that the radiation source term can be determined locally only by emission. With the assumption of optically thin limit, the radiative loss rate per unit volume can be expressed as :

$$Q_{rad}(T,\ Y_k)=4\sigma\sum(P_k\cdot a_{P,k})(T^4-T_b^4) \quad (17)$$

where σ is the Stefan-Boltzmann constant, P_k the partial pressure of species k, T the local flame temperature and T_b the background temperature. The Planck mean absorption coefficients $a_{P,k}$ for radiating species k such as H_2O, CO, and CO_2 are calculated from the curve fits recommended by TNF workshop (see TNF workshop web site).

2.3 Thermal NO formation

For H_2/CO-air flames at atmospheric pressure, only the thermal NO pathway is involved in the NO formation process and described by the extended Zeldovich mechanism. With the steady-state assumption for N atom and $[NO]/NO]_{equilibrium} \ll 1$, the thermal NO formation can be expressed as:

$$w_{NO}=M_{NO}(2K_{f9}[N_2][O]) \quad (18)$$

with $K_{f9}=1.84\times10^{14}\ \exp(-38370/T)\ cm^3/mol\text{-}s$.

Figure 2(a) gives the f-r plane data base of the NO formation rate at adiabatic condition ($e=1$) for the same flame condition as in Fig. 1. The maximum NO formation rate in the f axis occurs near the stoichiometric mixture fraction. The peak value in the r axis is located at $r=0.95$ where 5 % are deviated from the equilibrium state ($r=1$). The superequilibrium NO formation rate at $r=0.95$ is larger than the equilibrium one. This NO formation tendency in the f-r plane results from the strong dependency of the NO formation rate on temperature and mass fraction of O radical. As shown in Fig. 1, with increasing deviation from an equilibrium, the temperature decreases and concentration of O radical increases. Thus the NO formation rate is mainly governed by the opposing distribution trend of temperature and O radical. Figure 2(b) shows the f-e plane data base of the NO formation rate at $r=0.95$. The computed results indicate that the NO formation rate significantly decreases with increasing radiative heat loss due to the strong dependence of NO formation on temperature.

Due to the very low level of NO concentration and the quite long characteristic time scale of NO chemistry, any influences of NO formation on the combustion chemistry are neglected. Thus, the present model calculates the thermal NO in a post-processing step.

2.4 Turbulent combustion model

To account for the effects of turbulent fluctua-

tion on the thermochemical properties such as reaction rates, temperature, and species concentration, the Favre-averaged properties of the reacting mixture are evaluated by convoluting the instantaneous properties with the joint probability distribution:

$$\tilde{\phi}=\int_0^1\int_0^1\int_0^1\phi(f,\ r,\ e)\ \tilde{P}(f,\ r,\ e)dfdrde \tag{19}$$

$$\bar{\phi}=\bar{\rho}\int_0^1\int_0^1\int_0^1\frac{\phi(f,\ r,\ e)}{\rho(f,\ r,\ e)}\tilde{P}(f,\ r,\ e)dfdrde \tag{20}$$

where, the mean density is given by

$$\bar{\rho}=\left[\int_0^1\int_0^1\int_0^1\frac{\tilde{P}(f,\ r,\ e)}{\rho(f,\ r,\ e)}dfdrde\right]^{-1} \tag{21}$$

Mixture fraction f, reaction progress variable r, and enthalpy variable e are assumed to be statistically independent, so that the assumed joint probability density function (pdf) can be constructed as

$$\tilde{P}(f,\ r,\ e)=\tilde{P}(f)*\tilde{P}(r)*\tilde{P}(e) \tag{22}$$

The shape of pdf for the mixture fraction f is assumed to be the beta function.

Among three variables, the mixture fraction is the most important combustion scalar because it determines the mixing state of the turbulent flame fields. A small change in mixture fraction results in a large influence on temperature and species concentrations. On the other hand, the shapes of pdf for reaction progress variable r and enthalpy variable e have the negligibly small influence on the calculation (Janicka, 1982; Louis, 1997). In the present RPV-based joint pdf model, the shapes of pdf for r and e are assumed to be single delta function.

$$\tilde{P}(r)=\delta(r-\tilde{r})\ \text{and}\ \tilde{P}(e)=\delta(e-\tilde{e}) \tag{23}$$

For solution of the turbulent nonpremixed flame field, the governing equations include Navier-Stokes equations and additional scalar transport equations such as the turbulent kinetic energy, the dissipation of turbulent kinetic energy, the first- and second-order moments of mixture fraction, reaction progress variable, enthalpy variable, and the NO mass fraction. The detailed formulations for these governing transport equations are given in Table 2. To predict the global flow structure correctly in the bluff-body stabilized turbulent flames, a modified k-ε turbulence model is used here, where the model constant C_{ε_1} is changed from 1.44 to 1.60 as proposed by TNF workshop (TNF workshop web site). The source terms for the transport equation of mean reaction progress variable consist of four terms. As pointed in the previous work (Louis, 1997), the second and third terms arising from the nonadiabatic flame condition contribute only marginally. Decrease in the reaction progress variable is mainly governed by the first term. The expression $(1/W)(\partial^2 W/\partial f^2)$ included in this term has a negative maximum value at the stoichiometric mixture fraction. Thus, the first term

Table 2 Governing Transport Equations

$$\frac{\partial}{\partial t}(\rho\phi)+\frac{\partial}{\partial x_j}(\rho u_j\phi)=\frac{\partial}{\partial x_j}\left(\Gamma_\phi\frac{\partial\phi}{\partial x_j}\right)+S_\phi$$

φ	Γ_φ	S_φ
1	0	0
$\tilde{u}_i$	μ_{eff}	$-\frac{\partial\bar{p}}{\partial x_i}+\frac{\partial}{\partial x_j}\left(\mu_{eff}\frac{\partial\tilde{u}_j}{\partial x_i}\right)-\frac{2}{3}\frac{\partial}{\partial x_i}\left(\mu_{eff}\frac{\partial\tilde{u}_j}{\partial x_j}\right)$
$\tilde{k}$	$\frac{\mu_{eff}}{\sigma_k}$	$G_k-\bar{\rho}\tilde{\varepsilon}$
$\tilde{\varepsilon}$	$\frac{\mu_{eff}}{\sigma_\varepsilon}$	$(C_{\varepsilon_1}G_K-C_{\varepsilon_2}\bar{\rho}\tilde{\varepsilon})\frac{\tilde{\varepsilon}}{k}$
$\tilde{f}$	$\frac{\mu_{eff}}{\sigma_f}$	0
$\tilde{g}$	$\frac{\mu_{eff}}{\sigma_g}$	$C_{g_1}G_g-C_{g_2}\bar{\rho}\tilde{g}\frac{\tilde{\varepsilon}}{k}$
$\tilde{r}$	$\frac{\mu_{eff}}{\sigma_r}$	$C_g\bar{\rho}\tilde{\gamma}\left(\frac{\tilde{W}_{ff}}{W}+(1-\tilde{e})\frac{\tilde{U}_{ff}}{U}\frac{\tilde{W}_e}{W}\right)\tilde{g}\frac{\tilde{\varepsilon}}{k}+\tilde{r}\frac{\overline{W_e}}{W}S_e+\bar{S}_r$
$\tilde{e}$	$\frac{\mu_{eff}}{\sigma_e}$	$(\tilde{e}-1)C_g\frac{\tilde{U}_{ff}}{U}\bar{\rho}\tilde{g}\frac{\tilde{\varepsilon}}{k}-\bar{S}_e$
$\bar{Y}_{NO}$	$\frac{\mu_{eff}}{\sigma_s}$	$\overline{w_{NO}}$

$\tilde{g}=\widetilde{f''^2}$, $C_g=1.0$, $C_{g_1}=2.0$, $C_{g_2}=2.0$

$\sigma_f=\sigma_r=\sigma_e=\sigma_s=0.85$, $\sigma_g=0.9$

$$G_k=\mu_t\left\{\frac{1}{2}\left(\frac{\partial u_j}{\partial x_i}+\frac{\partial u_i}{\partial x_j}\right)^2-\frac{2}{3}\left(\frac{\partial u_k}{\partial x_k}\right)^2\right\}$$

$$G_g=\frac{\mu_t}{\sigma_f}\frac{\partial\tilde{f}}{\partial x_j}\frac{\partial\tilde{f}}{\partial x_j},\ W(f,\ e)=Y_{H_2}{}^{eq}-Y_{H_2}{}^{ub}$$

$$U(f)=h_{ad}-h_{min},\ S_r=\frac{w^*_{H_2}}{W},\ S_e=\frac{Q_{rad}}{U}$$

represents the deviation from an equilibrium due to turbulence-chemistry interaction in the region where mixture close to the stoichiometry is subjected to turbulent mixing. And the final term including the three-body recombination reaction rate expressed in Eq. (2) causes the mixture to approach equilibrium. Therefore, the HO_2/H_2O_2 chemistry acts on this final source term by yielding the extra reaction path. As a result, the inclusion of the HO_2/H_2O_2 chemistry influences the flame field only through the transport equation of reaction progress variable while it has little effect on the lookup table database.

3. Numerical Model

The governing equations are discretized by the finite volume method with a TVD type high-order upwind scheme for convection terms and the central differencing scheme for diffusion terms. The non-staggered grid arrangement is used and PWIM (pressure weighted interpolation method) is adopted to prevent a pressure oscillation. Pressure-velocity coupling is handled by PISO algorithm. More detailed informations can be found elsewhere (Kim, 1994).

4. Results and Discussion

The burner has a bluff-body diameter, D_B= 50mm and fuel jet diameter, D_J=3.6mm. Fuel consists of 66.67% H_2 and 33.33% CO by volume, and the stoichiometric mixture fraction and the adiabatic flame temperature are 0.1350 and 2400K, respectively. Three flame conditions (HC1 flame, HC2 flame, and HC3 flame) for the H_2/CO bluff-body burner are listed in Table 3. The co-flow air velocity is set to 40m/s and the fuel jet has three different velocities, 134 m/s (HC1 flame), 321 m/s (HC2 flame), and 536 m/s (HC3 flame).

Table 3 Flame conditions for the H_2/CO bluff-body flames

CASE	Fuel Vel. UJ (m/s)	Renolds No. (ReJ)	% BO	T_{in} [K]
HC1	134	17,500	18	298
HC2	321	41,990	43	298
HC3	536	70,120	74	298

To ensure the grid-independent solutions, 150×100 nonuniform grid system is used for the computational domain which extends axially to $X/D_B=10$ and radially to the outer radius (0.1 m). The fully developed condition is imposed on the outlet and the free stream condition is specified at the open boundary. The inlet boundary conditions of axial velocity and turbulent kinetic energy at the fuel jet and the coflow air stream are taken from the measured data (Masri, 1996; Combustion data base). The inlet dissipation rate is estimated with the formula for the turbulent length scale.

Three flames investigated in this study are classified as the fuel-jet dominant flame where fuel jet with higher momentum flux continuously penetrates into the recirculation zone formed behind the flame holder and passing by the neck zone, followed by a long, jet-like flame at the further downstream region (Masri, 1996). The neck zone in the bluff-body stabilized flame field is located downstream of the recirculation zone. In this neck zone, the turbulent mixing is intense and flame blow-off possibly occurs at sufficiently high flow velocities. In the present study, effect of the fuel jet velocities on flame structure and NOx formation is numerically analyzed. Since the HC2 flame and HC3 flame with the higher fuel jet velocity have the quite similar flame structure, the detailed discussions are made only for the HC1 flame and HC2 flame. Figure 3 shows the predicted streamlines and temperature fields for two flames (HC1, HC2). It can be clearly seen that there exists a distinctly different flow pattern and flame structure between two flames. In case of the lower fuel-jet velocity flame (HC1 flame), an inner vortex near the central fuel jet is formed and the large portion of fuel is transported from the inner vortex to the outer vortex. In case of the higher fuel-jet velocity flame (HC2 flame), the jet momentum flux is considerably increased so that the inner vortex nearly disappears, and most of fuel penetrates along the centerline and passes

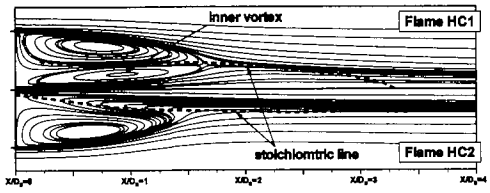

(a) Streamlines

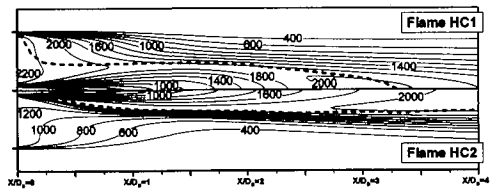

(b) Temperature

Fig. 3 Predicted steamlines and temperature contours for the HC1 flame and the HC2 flame

downstream without being transported to the outer vortex. The stoichiometric lines represented by the dotted lines characterize the different mixing pattern of two flames. The stoichiometric line for the HC1 flame is placed along the edge of the outer vortex. For the HC2 flame, the stoichiometric line is located along the edge of the central fuel jet. Consequently, the corresponding flame structure for two flames becomes quite different in the proximity of the outer core vortex zone. The predicted temperature field reveals that the HC1 flame has a visible flame within the outer vortex due to sufficient fuel transportation for creating a flammable mixture, while the HC2 flame does not. This predicted flame structure is consistent with the experimental observation (Masri, 1996). It is also expected that the existence or disappearance of the visible flame in the outer vortex plays an important role in the NO formation characteristics and flame stabilization.

In order to separately address the effects of nonequilibrium chemistry and radiative heat transfer on the flame structure and the NO formation, the detailed comparison between prediction and measurement has been made for the HC1 flame. In the following plots, Model 1 and 2 represent the RPV turbulent combustion model without and with considering HO_2/H_2O_2 chemistry effect, respectively. Figure 4 presents the com-

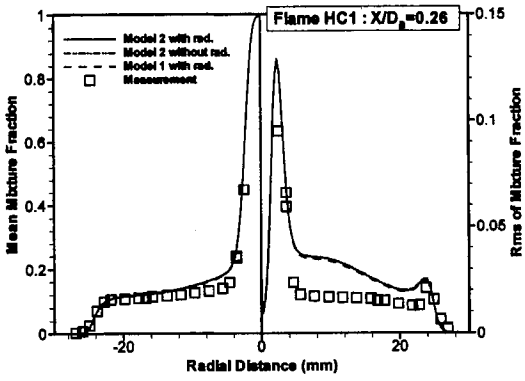

Fig. 4 Radial profiles of mean and rms of mixture fraction at $X/D_B=0.26$ for the HC1 flame

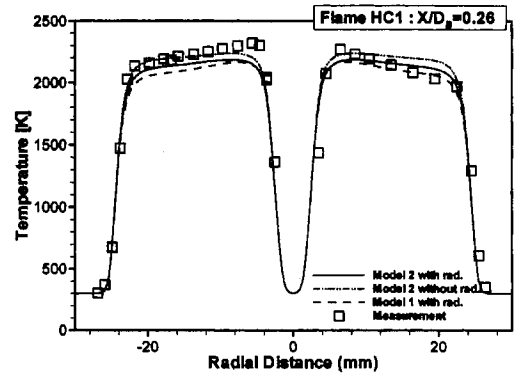

Fig. 5 Radial profiles of mean temperature at $X/D_B=0.26$ for the HC1 flame

parison of predicted and measured radial profiles of mean and rms fluctuation of mixture fraction at axial location ($X/D_B=0.26$) within the recirculation zone. The core of outer vortex has a nearly uniform distribution of mean mixture fraction that is close to the stoichiometric condition ($f_{st}=0.1350$). The modified turbulence model with $C_{\epsilon_1}=1.60$ used here yields the correct prediction of mean mixture fraction, but still overpredicts the variance of mixture fraction. The overpredicted mixture fraction variance leads to the underpredicted temperature distribution due to the larger concentration fluctuations. As shown in Fig. 4, the mixture fraction field is almost insensitive to the effects of HO_2/H_2O_2 chemistry and radiative heat loss.

The temperature profiles displayed in Fig. 5 indicate that, within the outer vortex, the HC1 flame has the visible flame zone higher than

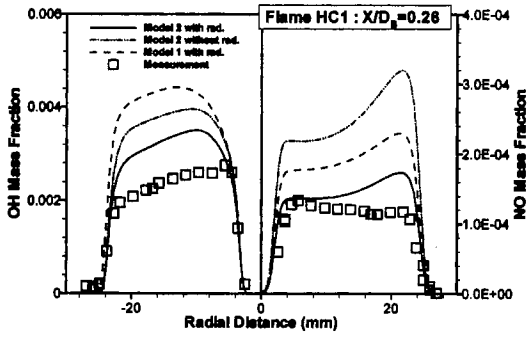

Fig. 6 Radial profiles of OH and No mass fractions at $X/D_B=0.26$ for the HCl flame

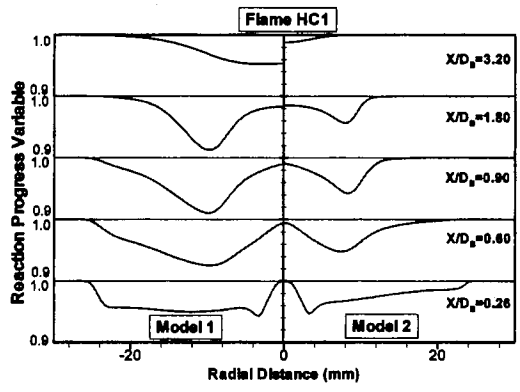

Fig. 7 Effects of HO_2/H_2O_2 chemistry on distribution of reaction progress variable for thr HCl flame

2100K. The significant radiative cooling in this high-temperature zone leads to the decrease of flame temperature roughly by 100 K. Compared to Model 1, Model 2 predicts the higher temperature because the HO_2/H_2O_2 chemistry included in Model 2 yields the extra reaction path which reduces the deviations from equilibrium. But, all models underpredict the mean temperature due to defect of the turbulence model which still overpredicts the mixture fraction variance. Figure 6 shows the radial profiles of mass fraction for OH and NO at X/DB=0. 26. The effect of nonequilibrium chemistry and radiation substantially influences the superequilibrium concentrations of free radicals and NO formation. By considering the radiation effect, temperature and mass fraction of OH and NO are almost linearly decreased. Model 1 overpredicts the superequilibrium concentration of OH radical. The unacceptably high level of radical concentration predicted by Model 1 is mainly caused by the neglect of the HO_2/H_2O_2 chemistry. Thus the omission of HO_2/H_2O_2 chemistry underpredicts the recombination of free radicals, and the larger departure from the equilibrium condition is leading to the overprediction of super-equilibrium radical concentrations. Consequently the Model 1 predicts the highest NO concentration because the increase in the superequilibrium O radical concentration increases the NO formation rate by attacking the strong N2 bond. There exist the quantitative differences with prediction and measurement and these discrepancies might be mainly attributed to the defect of turbulence model and combustion model, and the neglect of convective heat loss at the wall. The larger departure from the equilibrium state predicted by Model 1 can be confirmed by the radial distributions of reaction progress variable shown in Fig. 7. As mentioned above, the reaction progress variable is a measure of the deviation from equilibrium and its decrease is almost contributed by the second source term listed in Table 2. The significant deviation from equilibrium appears within the recirculation zone where the nearly stoichiometric mixture fraction is distributed. With passing through the neck zone, the deviation occurs along the reaction shear layer near the edge of the fuel central jet. At the further downstream flame region having the much lower turbulent mixing rate, the combustion processes gradually reach to the equilibrium state. Compared to Model 1, Model 2 accounting for the HO_2/H_2O_2 chemistry predicts much faster decay of the radical pool and the corresponding combustions are proceeding with relatively small departure from equilibrium.

Figure 8 shows the radial profiles of mean H_2O mass fraction and temperature at $X/D_B=1.8$ near the neck zone. The effects of nonequilibrium chemistry and radiation have little influence on the prediction of major species. Model 2 predicts the peak temperature higher than Model 1 roughly by 100K while the radiative heat loss has the negligibly small influences on the mean temperature. As shown in Fig. 9, OH profile predicted by Model 2 agrees well with the experimental data,

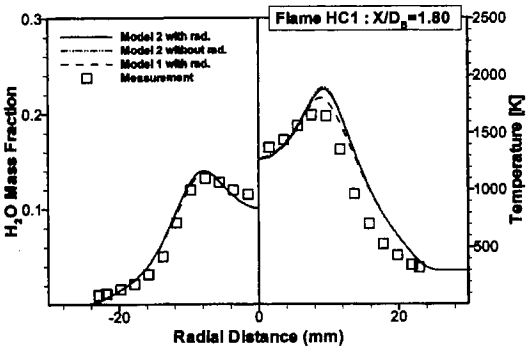

Fig. 8 Radial profiles of H_2O mass fraction and mean temperature at $X/D_B=1.80$ for the HC1 flame

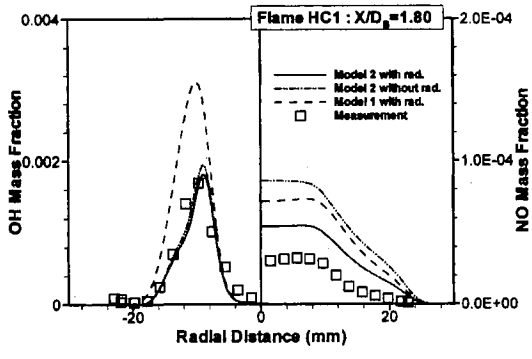

Fig. 9 Radial profiles of OH and NO mass fractions at $X/D_B=1.80$ for the HC1 flame

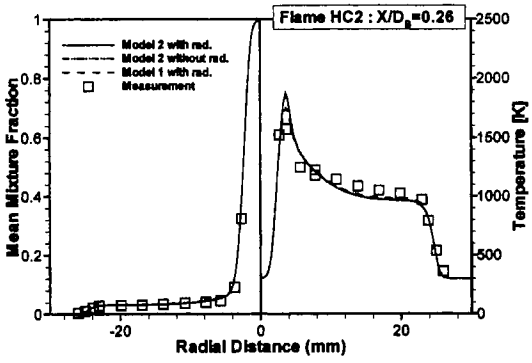

Fig. 10 Radial profiles of mean mixture fraction and mean temperature at $X/D_B=0.26$ for the HC2 flame

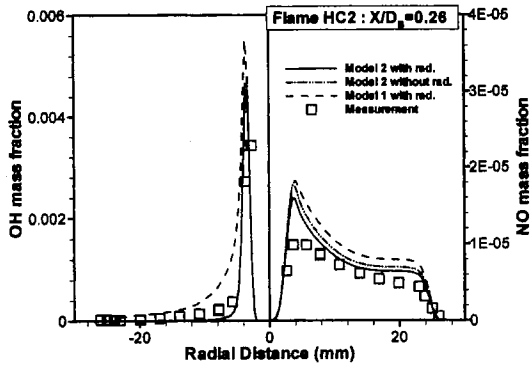

Fig. 11 Radial profiles of OH and NO mass fractions at $X/D_B=0.26$ for the HC2 flame

but NO level is overpredicted.

Next, for further assessment of the present RPV combustion model, the detailed comparison between prediction and measurement has been made for the higher fuel jet velocity case (HC2 Flame). Figure 10 gives the comparison of predicted and measured radial profiles of mean mixture fraction and temperature at $X/D_B=0.26$. Compared to HC1 flame, HC2 flame forms the much leaner mixture which is uniformly distributed in the outer vortex. Therefore, the corresponding temperature is much lower than one of HC1 flame due to the absence of flame. In the outer vortex region with the much leaner and lower temperature mixture, the effects of nonequilibrium chemistry and radiative heat loss are considerably suppressed. Figure 11 shows the radial profiles of mass fraction for OH and NO at $X/D_B=0.26$. The narrow distribution of OH radical implies that the reaction site is created only at the shear layer along the central jet. The NO level formed at $X/D_B=0.26$ is an order of magnitude smaller than that of the HC1 flame.

Finally, to investigate the effect of fuel jet velocities on the NO formation characteristics, a new NO index (NOI) is defined as the net mass of NO convected downstream per unit mass of jet fuel at a given axial location. As shown in Fig. 12, there is a substantial difference in NO formation characteristics between the lower fuel jet velocity case (HC1) and the higher fuel jet velocity cases (HC2 and HC3). For HC1 flame, in the high temperature recirculation, most of NO formation occurs and NOI increases abruptly. For HC2 flame and HC3 flame with the higher fuel jet velocity, little NO forms within the nearly nonreacting recirculation zone and NO formation continuously takes place along the jet-like flame at further downstream location of the neck zone.

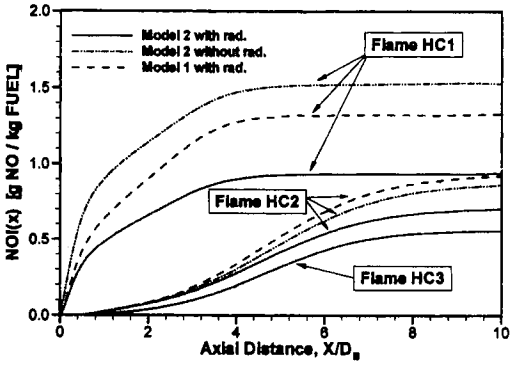

Fig. 12 Predicted axial distributions of the NOx emission for the three fuel jet velocities; 134m/s (HC1), 321m/s(HC2), and 536m/s (HC3)

The numerical results obtained from three turbulent combustion models indicate the effects of nonequilibrium chemistry and radiative heat loss are quite crucial for the prediction of NO emission especially in the lower fuel jet velocity flame (HC1).

5. Conclusions

(1) The present turbulent combustion model correctly predicts the essential features of flame structure and NO formation in the H_2/CO-air bluff-body stabilized flames, and the numerical results reasonably well agree with experimental data in terms of mean flame temperature, concentration of major species and radical, and NO concentration.

(2) The reaction progress variable approach including the additional HO_2 and H_2O_2 chemistry can successfully account for the nonequilibrium chemistry effect on the nonpremixed turbulent flame. The neglect of HO_2 and H_2O_2 chemistry underpredicts the recombination of free radicals, and the larger departure from the equilibrium condition is leading to the overprediction of super -equilibrium radical concentrations and NO formation.

(3) In the H_2/CO-air bluff-body stabilized flames, the lower (HC1) and higher (HC2) fuel -jet velocity flames have the quite different flame structures in proximity of the outer core vortex zone. The HC1 flame has a visible flame within the outer vortex while HC2 flame does not. The existence of visible flame in the outer vortex is a crucial element for NO formation characteristics and flame stabilization.

(4) For HC1 flame, most of NO formation occurs in the recirculation zone due to the high flame temperature and therefore NOI increases abruptly in this region. In the case of the higher flame conditions (HC2, HC3), little NO forms due to the absence of flame within the recirculation zone and NO formation continuously takes place along the jet-like flame at further downstream location of the neck zone.

References

Biagioli, F., 1997, "Comparison between Presumed and Monte Carlo Probability Density Function Combustion Models," *Journal of Propulsion and Power*, Vol. 13, No. 1, pp. 109~116.

Combustion data base, http://www. mech. eng. usyd. edu. au/research/energy/#data, The University of Sydney and the combustion research facility, Sandia National Laboratories,

Computation of Bluff-Body Stabilized Jets and Flames, Section 4, TNF Workshop Proceedings, *Third International Workshop on Measurement and Computation of Turbulent Nonpremixed Flames*, Boulder, Colorado, 1998.

Correa, S. M., Drake, M. C., Pitz, R. W., and Shyy, W., 1984, "Prediction and Measurement of a Non-Equilibrium Turbulent Diffusion Flame," *Proc. 20th Symp. (Int.) Comb.*, Combustion Institute, Pittsburgh, p. 337.

Correa, S. M. and Pope, S. B., 1994, "Raman Measurements and Joint PDF Modeling of a Nonpremixed Bluff-Body-Stabilized Methane Flame," *Proc. 25th Symp. (Int.) Combl., Combustion Institute, Pittsburgh, p. 1167.*

Janika, J. and Kollmann, W., 1982, "The Calculation of Mean Radical Concentrations in Turbulent Diffusion Flames," *Combustion and Flame*, Vol. 44, pp. 319~336.

Kim, Y. M., Shang, H. M., Chen, C. P., and Wang, T. S., 1994, "Prediction of Confined Swirling Spray-Combusting Flows," *Numerical Heat*

Transfer, Vol. 25, pp. 1~20.

Kok, J. B. W. and Louis, J. J. J., 1998, "Modeling Turbulent Combustion in a CO/H_2 Diffusion Flame Using Reaction Progress Variables," *Combust. Sci. and Tech.*, Vol. 131, p. 225.

Louis, J. J . J., 1997, "On Turbulent Combustion of Coal Gas," PhD. Thesis, Univ. of Twente, Enschede.

Masri. A. R.. Dibble. R. W.. and Barlow. R. S.. 1996, "The Structure of Turbulent Nonpremixed Flames Revealed by Raman-Rayleigh-LIF Measurements," *Progr. Energy Combust. Sci.*, Vol. 22, pp. 307~362.

TNF workshop web site, http://www. ca. sandia. gov/tdf/Submodels. htm

Warnatz, J., Maas, U., and Dibble, R. W., 1996, *Combustion*, Springer-Verlag, Berlin, Germany.